Letter

Rashba-type splitting of the Au(110) surface state: A combined inverse and direct photoemission study

Katharina T. Ritter [1,*] Koji Miyamoto [2] Taichi Okuda [2] and Markus Donath [1,†]

[1] *Physikalisches Institut, Westfälische Wilhelms-Universität Münster, Wilhelm-Klemm-Straße 10, 48149 Münster, Germany*

[2] *Hiroshima Synchrotron Radiation Center, Hiroshima University, 2-313 Kagamiyama, Higashi-Hiroshima 739-0046, Japan*

(Received 19 July 2021; revised 10 September 2021; accepted 13 September 2021; published 4 October 2021)

The Shockley surface state located at $\overline{\mathrm{Y}}$ on the (1×2)-reconstructed Au(110) surface is predicted to exhibit a Rashba-type spin splitting. Previous photoemission experiments searched for this splitting but it could not be resolved yet. In order to uncover a possible splitting, the unoccupied surface state on Au(110) is examined with spin- and angle-resolved inverse photoemission, whereas Na-covered Au(110) allows for investigation of the now occupied surface state by means of spin- and angle-resolved direct photoemission. Our data show clear spin splittings in the order of 100 meV with a sign reversal at $\overline{\mathrm{Y}}$ in the surface state's in-plane spin components which is characteristic for a Rashba-type behavior. Furthermore, we deduce an effective mass of $m^* = (0.27 \pm 0.02)m_e$ and a Rashba parameter of $\alpha_R = (0.46 \pm 0.04)$ eV Å from direct photoemission measurements.

DOI: 10.1103/PhysRevB.104.L161101

I. INTRODUCTION

The Au(111) Shockley surface state located in the L gap around $\overline{\Gamma}$ is the prototypical state for a Rashba-type spin splitting [1–4]. Similarly, the surface-projected L gap exists on Au(110), yet is centered around the $\overline{\mathrm{Y}}$ point. Here, the band gap also features a surface state [5–7]. Due to the C_{2v} symmetry of the (110) surface the dispersion of the surface state is anisotropic. On the unstable unreconstructed (1×1) surface, this surface state is occupied and was observed by Nuber *et al.* [8] employing angle-resolved photoemission spectroscopy (ARPES). However, at room temperature a stable (1×2) or *missing-row* reconstruction is found [9–13] and—in contrast to a (1×1) surface—the surface state is unoccupied. Its dispersion has been investigated with angle-resolved inverse photoemission (IPE) [14,15]. Na deposition shifts the surface state below the Fermi level E_F without changing the (1×2) reconstruction, and thereby making it accessible for direct photoemission experiments [8].

The mere existence of the Au(110) surface state remains unchallenged. However, experimental evidence for a Rashba spin splitting is lacking [8,14,15]. Nevertheless, various calculations predict an anisotropic Rashba splitting of the Au(110) surface state [8,16,17]. Within the simple Rashba model, the spin degeneracy of a parabolic dispersing surface state is lifted, thereby introducing an energetic shift of the two parabolas linear in $k_\parallel$. Its dispersion, for Au(110) around $\overline{\mathrm{Y}}$, yields $E(k_\parallel) = \frac{\hbar^2}{2m^*}k_\parallel^2 \pm \alpha_R|k_\parallel| + E_0$, where m^* is the effective mass, $\alpha_R = \frac{\hbar^2}{2m^*}|\Delta k_\parallel|$ is the Rashba parameter ($\Delta k_\parallel$ marks the displacement between the band minima), and E_0 is the energy at which the two parabolas intersect (or band minimum for the spin-integrated case). Table I provides an overview of the parameters found or predicted for Au(110) along $\overline{\Gamma}\,\overline{\mathrm{Y}}\,\overline{\Gamma}$, where the Rashba splitting is expected to be larger than along $\overline{\mathrm{S}}\,\overline{\mathrm{Y}}\,\overline{\mathrm{S}}$ [17]. Notably, the experimental results suggest the effective mass to be larger than calculated. Nevertheless, the Rashba splitting remains unreported from an experimental point of view.

In this Letter, we address the Rashba splitting of the Shockley surface state on the (1×2)-reconstructed Au(110) surface along $\overline{\Gamma}\,\overline{\mathrm{Y}}\,\overline{\Gamma}$. By combining inverse and direct photoemission experiments, we are able to investigate (i) the unoccupied surface state on Au(110) with spin- and angle-resolved IPE, and (ii) its occupied variant on Na-covered Au(110) with (spin-resolved) (S)ARPES. The splitting of the surface state can already be observed in our spin-integrated ARPES data. Spin-resolved measurements (IPE and SARPES) confirm the Rashba-type nature of the splitting as the in-plane spin components are reversed when crossing the $\overline{\mathrm{Y}}$ point. This allows us to determine the characteristic parameters of the surface state's Rashba behavior on Au(110) from experimental data.

II. EXPERIMENTAL DETAILS

In order to prepare a pristine surface, the Au(110) single crystals (grown and polished by MaTeck GmbH) were precleaned using cycles of Ar^+ bombardment (0.6–1 kV) and annealing up to 450 °C. A well-ordered surface was achieved for a brand new crystal after approximately 50 sputter and anneal cycles. Between measurements a clean surface was restored by a two-step preparation: (i) Ar^+ bombardment at $T_\mathrm{sample} = 200$ °C and subsequent annealing at $T_\mathrm{sample} = 450$ and 200 °C, followed by (ii) Ar^+ bombardment at room temperature and annealing at $T_\mathrm{sample} = 450$ and 200 °C. Lowering the annealing temperature to 200 °C assists to obtain a well-ordered reconstruction. Na was evaporated from a dispenser

*ritter.katharina@uni-muenster.de

†markus.donath@uni-muenster.de

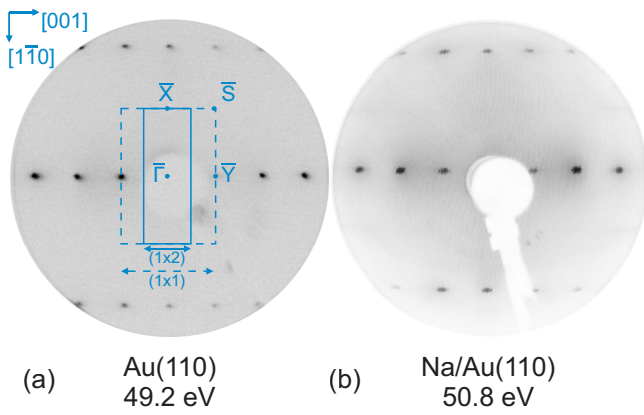

FIG. 1. LEED patterns of the Au(110) (a) and Na/Au(110) (b) surfaces show the (1×2) superstructure caused by a "missing-row" reconstruction. The surface Brillouin zone of the (1×2) surface is marked with solid lines, the (1×1) in dashed lines.

(SAES Getters) onto the sample at room temperature. This leads to electron doping which lowers the sample's work function and shifts the surface state below the Fermi level. The low-energy electron diffraction (LEED) patterns in Figs. 1(a) and 1(b) indicate a well-ordered (1×2)-reconstructed surface after preparation for Au(110) and Na/Au(110), respectively. Auger electron spectroscopy showed no indication of surface contamination, especially no carbon. In accordance with this, the surface state around $\bar{Y}$ was clearly visible during data acquisition. From target current spectroscopy we obtained a work function of $\Phi_{\mathrm{Au(110)}} = (5.25 \pm 0.05)$ eV which is in good agreement with the literature [18].

Spin- and angle-resolved inverse photoemission measurements were realized in Münster, Germany [19]. A beam of spin-polarized electrons (spin polarization 29%) emitted from a GaAs photocathode was guided at a defined angle of incidence θ onto the sample matching the in-plane (P_y) spin component perpendicular to $k_\parallel$. The emitted VUV photons were detected with acetone-filled photon detectors (CaF_2 window) operating in proportional counting mode [20]. The mean energy of the optical bandpass yields $\hbar\omega = 9.9$ eV. Measurements were carried out at $T_{\mathrm{sample}} = 292$ K and at base pressure $<1\times10^{-10}$ mbar. The energy resolution was 450 meV [21] and the angular resolution $\Delta\theta \pm 2^\circ$ [22].

The direct photoemission measurements on Na/Au(110) were performed at the BL-9B end station of the Hiroshima Synchrotron Radiation Center (HiSOR), Japan, using p-polarized light of $\hbar\omega = 21$ eV. At this photon energy the surface state appeared with high intensity. Spin-integrated photoelectrons were analyzed in a hemispherical analyzer (VG Scienta R4000) and detected with a microchannel plate (MCP). The in-plane (Rashba) spin component (P_y) of the photoelectrons was detected by the ESPRESSO machine [23,24]. The very low-energy electron diffraction (VLEED)-type spin-polarization detector had a Sherman function of $S = 0.15$. All measurements were carried out at $T_{\mathrm{sample}} = 50$ K and at base pressure $<2\times10^{-10}$ mbar. The energy and angular resolutions were $\Delta E = 37$ meV and $\Delta\theta = \pm0.3^\circ$ for ARPES, and $\Delta E = 65$ meV and $\Delta\theta = \pm3^\circ$ for SARPES.

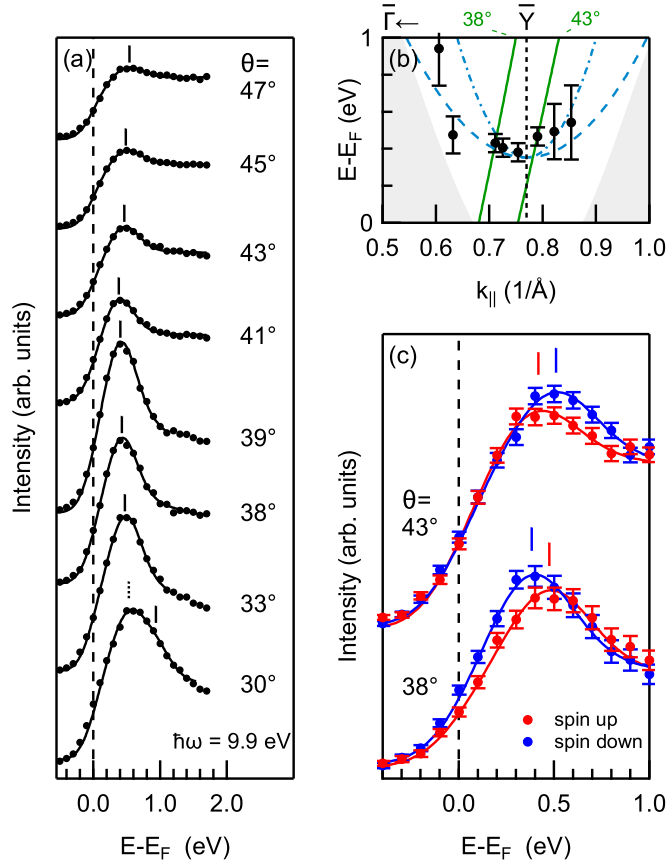

FIG. 2. Spin- and angle-resolved inverse photoemission data around $\bar{Y}$ on (1×2)-Au(110): (a) Spin-integrated spectra exhibit the dispersing Rashba-type surface state (black tick marks) and a bulk transition (dashed tick mark). (b) Dispersion $E(k_\parallel)$ of the surface state as derived from peak positions in (a) located in the band gap around $\bar{Y}$. Blue lines resemble the dispersions published in Refs. [14] (dashed) and [16] (dotted-dashed). Surface-projected band structure (light gray area) taken from Ref. [15]. Spin-resolved spectra were measured for $\theta = 38^\circ, 43^\circ$ (green solid lines). (c) Reversal of sign in the spin signal for spectra taken left and right of $\bar{Y}$ ($\theta_{\bar{Y},E_f=0.35\,\mathrm{eV}} = 42.3^\circ$) confirms the Rashba splitting of the surface state. Spectra for spin up (spin down) of the P_y component are plotted in red (blue).

III. RESULTS AND DISCUSSION

A. IPE

The IPE measurements aim for revealing the Rashba splitting of the unoccupied surface state on (1×2)-Au(110). Figure 2 presents our IPE results. The spin- and angle-resolved IPE spectra were normalized to absorbed charge during data acquisition. Here, all intensities displayed are referenced to a common background intensity at $E - E_F = 3$ eV, thereby achieving comparability. The solid lines through the data points are obtained from curve fits using the following function, $F = A * [(1 - f)(L + B)]$ (see the Supplemental Material of Ref. [25]). We assume Lorentzian lines L added onto a background intensity B, which models secondary processes, multiply the results with the Fermi function for unoccupied states $(1 - f)$ at the given sample temperature, and finally convolute the results with a Gaussian apparatus

TABLE I. Characteristics of the surface state on Au(110) along $\overline{\Gamma}\,\overline{\mathrm{Y}}\,\overline{\Gamma}$.

Structure	Method	$E_0 - E_F$ (eV)	m^*/m_e	α_R (eV Å)	Ref.
(1×2)	IPE	0.3	0.3		[14]
(1×1)	IPE	0.7	0.20[a]		[15]
(1×2)	IPE	0.5[a]			[15]
(1×1)	ARPES	-0.590 ± 0.005	0.13 ± 0.01		[8]
(1×2)	*Ab initio* calculation	≈0.03[a]	0.10 ± 0.01[a]	≈0.76[a]	[16]
(1×1)	*Ab initio* calculation	−0.37	0.11	0.8	[17]

[a]Extracted from figure in reference.

function A to account for the energy resolution of the experiment [26].

Spin-integrated IPE spectra for various angles of electron incidence ($30^\circ \leqslant \theta \leqslant 47^\circ$) around $\overline{\mathrm{Y}}$ are shown in Fig. 2(a). The spectra are dominated by the surface state that appears as a sharp feature (solid tick marks) with a band minimum at $E - E_F = 0.35$ eV. This is in line with the findings of Bartynski and Gustafsson [14] ($E_0 = 0.3$ eV) and Drube *et al.* [15] ($E_0 = 0.5$ eV for the reconstructed surface). In addition, for the smallest angle $\theta = 30^\circ$ (and perhaps 33°), a bulk transition is mixed in, which similarly exists for related metal surfaces such as Ag(110) [27] or Cu(110) [28]. This leads to a broad asymmetric feature as seen in our 30° spectrum.

The dispersion $E(k_\parallel)$ of the surface state derived from the spectra is shown in Fig. 2(b). As the effective mass m^* varies throughout previous publications (see Table I), we plotted parabolas with the smallest ($0.1m_e$[16], blue dotted-dashed line) and largest value ($0.3m_e$ [14], blue dashed line) for reference by adapting their band minima to our band minimum. Deriving the exact effective mass from IPE data, however, remains challenging because of uncertainties associated with the peak positions due to (i) the effective energy resolution and (ii) the bulk transition observed for $\theta = 30^\circ$. The first one is a consequence of the finite angular resolution that leads to an additional energy broadening of the observed electronic state if a single spectrum cuts a dispersion rather parallel. Moreover, the intensity of the surface state decreases drastically towards larger angles of incidence [29]. This adds to the limited accessibility of the branch for $k_\parallel \gtrsim 0.85$ Å^{-1}. Nevertheless, the surface state's dispersion as measured with IPE is in good agreement with the literature.

In order to reveal the Rashba-type splitting, we chose two exemplary angles left and right of the high symmetry point $\overline{\mathrm{Y}}$, i.e., $\theta = 38^\circ$ and 43° [green lines in Fig. 2(b)], and performed spin-resolved IPE measurements. Figure 2(c) shows the spin-resolved IPE spectra for both angles. The sign reversal for the Rashba-type spin component is clearly visible and the spin-dependent energy splitting is in the order of ≈100 meV. Below $\overline{\mathrm{Y}}$ the lower branch of the spin-split state has spin-down character while the upper branch has spin-up character. This behavior changes across $\overline{\mathrm{Y}}$ where now spin up marks the lower branch of the lifted degeneracy. It might be surprising that the spin-dependent energy splitting is about the same in the spectra for 38° and 43°, although the 43° spectrum probes the surface state closer to $\overline{\mathrm{Y}}$ than the 38° spectrum [see green lines in Fig. 2(b)]. Note that the spectra have been obtained for constant θ and not for constant $k_\parallel$. As a consequence, the constant-angle lines cut the $E(k_\parallel)$ dispersion of the surface state at different angles. Therefore, the measured spin-dependent energy splitting is smaller (larger) than the actual splitting at given $k_\parallel$ for θ below (beyond) $\overline{\mathrm{Y}}$. This explains the almost identical spin splittings in the spectra for 38° and 43°.

All in all, IPE data provide clear evidence of the Rashba splitting of the surface state located around $\overline{\mathrm{Y}}$ on (1×2)-Au(110).

B. ARPES

To complement and crosscheck our IPE results we make use of the high experimental resolutions available with direct photoemission techniques to investigate the very same surface state that shifts below the Fermi level upon doping with Na. Figure 3 presents the (S)ARPES results for the surface state on the Na-covered (1×2)-Au(110) surface along the $\overline{\Gamma}\,\overline{\mathrm{Y}}\,\overline{\Gamma}$ direction in the vicinity of $\overline{\mathrm{Y}}$. Please note that all angles and momenta now come with a negative sign because in our (S)ARPES setup the sample was rotated in the opposite direction compared with IPE. The occupied surface state as measured with ARPES is shown in a contour plot in Fig. 3(a). The Na coverage was chosen such that the surface state becomes clearly visible with a band minimum at $\overline{\mathrm{Y}}$ being located at $E - E_F = (-210 \pm 15)$ meV. The blue line indicates the surface state's dispersion with an effective mass of $m^* = (0.25 \pm 0.02)m_e$ as obtained from curve fitting the momentum distribution curves (MDCs) nearby E_F.

A more detailed picture arises from the corresponding energy distribution curves (EDCs). Figure 3(b) contains a series of EDCs for a selection of single slices for angles between -17.7° and -25.7° (each slice's angular width ≈ $0.08^\circ \ll$ angular resolution $\Delta\theta$). Interestingly, ARPES data already expose the existence of a splitting in the surface state: The rather sharp peak at $\overline{\mathrm{Y}}$ changes into an asymmetric feature consisting of two underlying states. By assuming two Lorentzian features and carefully applying the curve fit to the EDCs the energetic positions of the initial states are obtained (Lorentzian functions exemplarily shown for -23.2°). The resulting peak positions are marked in Fig. 3(b) accordingly. The curve fits for the peak positions translate to the open circles in the dispersion $E(k_\parallel)$ shown in Fig. 3(c). This allows for the determination of the effective mass and the Rashba parameter which are found to be $m^* = (0.29 \pm 0.01)m_e$ and $\alpha_R = (0.51 \pm 0.02)$ eV Å, respectively. The parabolic dispersions curve-fitted for both branches of the spin-split surface state

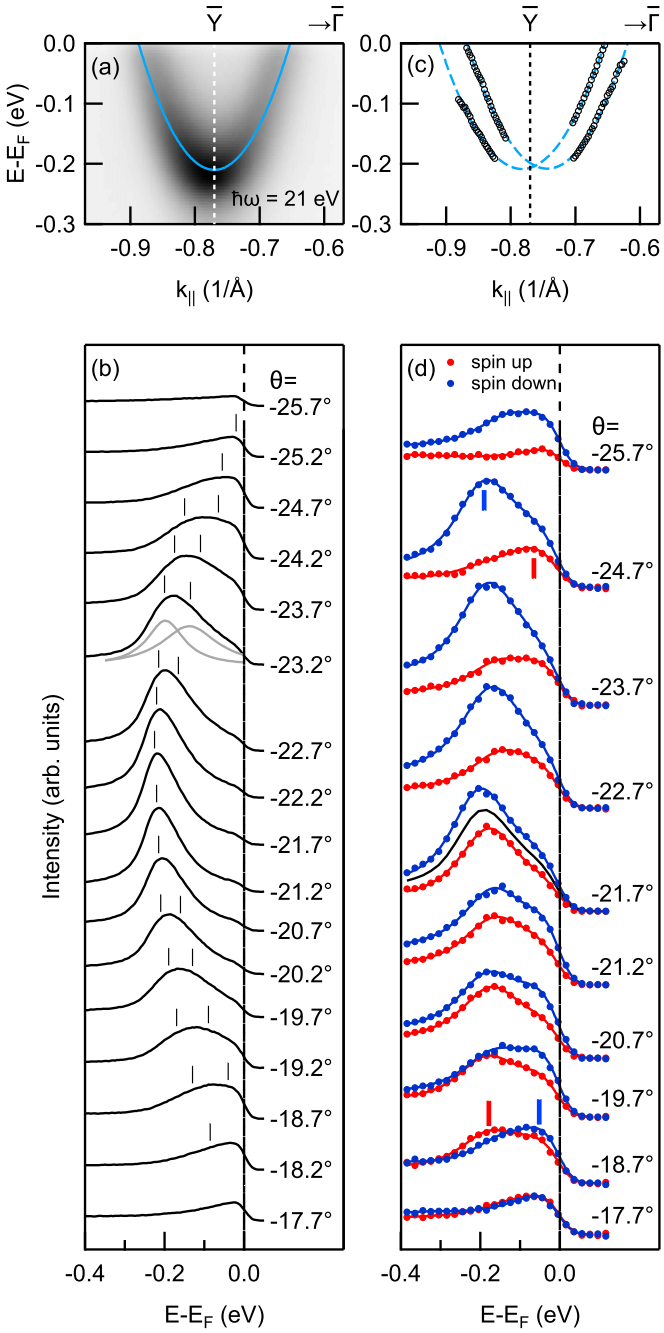

FIG. 3. Spin- and angle-resolved photoemission around $\overline{\mathrm{Y}}$ of Na-covered (1×2)-Au(110) measured with p-polarized light ($\hbar\omega = 21$ eV): (a) The intensity of the Rashba-type surface state mapped with ARPES is displayed as a contour plot (linear gray scale). Its dispersion is sketched by the blue solid line. (b) ARPES EDCs show the dispersion of the surface state (tick marks). Its Rashba-type spin splitting results in an asymmetric line shape away from $\overline{\mathrm{Y}}$. An example of the two-line-decomposition fit procedure is shown as gray lines for $\theta = -23.2°$. (c) Dispersion $E(k_\parallel)$ deduced from curve fitting the EDCs with two Lorentzian functions (open circles). The dispersion is fitted by two parabolas (blue dashed lines). (d) SARPES data confirm the sign reversal of the P_y spin component. Spectra for spin up (spin down) of the P_y component are plotted in red (blue). Peak positions are marked for two exemplary angles. The black solid line depicts the spin-averaged spectrum for $-21.7°$.

are shown in Fig. 3(c) as blue dashed lines. Their crossing at $k_\parallel = 0.76$ Å^{-1} and $E - E_F = -203$ meV complies with a band minimum deduced earlier from the EDCs (−210 meV at $\overline{\mathrm{Y}}$). In addition, the Rashba parameter is also derived from analyzing the MDCs which implies $\alpha_R = (0.41 \pm 0.04)$ eV Å. As already mentioned above, in this analysis the effective mass yields $m^* = (0.25 \pm 0.02)m_e$ while the parabolas' displacement $\Delta k_\parallel$ increases from 0.03 Å^{-1} (EDCs) to 0.04 Å^{-1} (MDCs). Both analyses combined, we find an effective mass of $m^* = (0.27 \pm 0.02)m_e$ and a Rashba parameter of $\alpha_R = (0.46 \pm 0.04)$ eV Å. The Rashba parameter on Na-covered (1×2)-Au(110) is found to be smaller than predicted for Au(110) [16,17].

The Rashba splitting has been established with ARPES and we now focus on resolving the surface state's spin components by performing SARPES measurements. For various angles between $-17.7°$ and $-25.7°$ the SARPES data are shown in Fig. 3(d). As in our spin-resolved IPE data, we also observe a strong spin dependence in the SARPES data. A comparison of the spectra for $\theta = -18.7°$ and $-24.7°$ evidences the sign reversal in the spin polarization: The $-18.7°$ spectrum shows the spin-down component closer to the Fermi level whereas at $-24.7°$ spin up has the lower binding energy. The succession of the spin components is expectedly inverted with respect to spin-resolved IPE data due to directions of sample rotation and thus confirms our previous results. We find the surface state to appear broader in SARPES than in ARPES as showcased by the spin-integrated $-21.7°$ SARPES spectrum [black solid line in Fig. 3(d)]. Due to the loss in intensity caused by spin resolution we chose intensity over angular resolution, which differs by a factor of 10 compared with the ARPES setup. A second consequence of the lower angular resolution is the increased intensity nearby the Fermi level in the SARPES data [30]. As an additional consequence, some peak positions in SARPES are slightly different from the ARPES results.

One more observation has to be discussed: Apart from the spin splitting, the spin-down intensities (blue) dominate the SARPES series independently of $k_\parallel$. The light incidence angle of 50° relative to the electron analyzer breaks the symmetry of the experiment. As a consequence for p-polarized light, spin-dependent intensities independent of $k_\parallel$ arise, which is known as a final state or matrix element effect in photoemission [31,32]. The observed spin polarization in the vicinity of the high symmetry point $\overline{\mathrm{Y}}$ (C_{2v} symmetry) can be explained as follows: According to the theoretical formulation of the matrix elements for photoemission [31], the finite spin polarization is caused by a mixing of p_x and p_z orbitals within the Rashba spin-split state. This mixing is in agreement with the model calculation presented by Simon *et al.* [17]. Their model suggests that the mixing between p_x and p_z orbitals causes the anisotropy of the Rashba-type surface state on Au(110). Note that a surplus of spin-down intensity is also visible in the spin-resolved IPE data shown in Fig. 2(c). The smaller spin polarization effect in IPE compared with SARPES is attributed to the detection of unpolarized light in IPE.

In summary, the Rashba-type behavior of the Au(110) surface state—already established qualitatively by our IPE data—was quantitatively confirmed by a comprehensive ARPES and SARPES study.

IV. CONCLUSION

We uncovered the Rashba-type spin splitting of the surface state located in the surface-projected band gap around $\overline{\mathrm{Y}}$ in $\overline{\Gamma}\,\overline{\mathrm{Y}}\,\overline{\Gamma}$ direction on the (1×2)-reconstructed surfaces of Au(110) and Na/Au(110). In a combined study employing both spin- and angle-resolved inverse and direct photoemission experiments we provide experimental evidence of the characteristic sign reversal in the spin components of the surface state on Au(110) along $\overline{\Gamma}\,\overline{\mathrm{Y}}\,\overline{\Gamma}$. High-resolution ARPES data for Na/Au(110) not only already suggested the lift of the degeneracy but also allowed for the determination of characteristic parameters, namely the effective mass and the Rashba parameter. From analyzing EDCs and MDCs, we find values of $m^* = (0.27 \pm 0.02)m_e$ and $\alpha_R = (0.46 \pm 0.04)$ eV Å for the effective mass and Rashba parameter, respectively.

ACKNOWLEDGMENTS

M.D. and K.T.R. gratefully acknowledge the hospitality of the Hiroshima Synchrotron Radiation Center. (S)ARPES measurements were performed with the approval of the HiSOR program advisory committee (Proposal No. 16BG027). We thank F. Schöttke for his support with the IPE measurements.

[1] S. LaShell, B. A. McDougall, and E. Jensen, Spin Splitting of an Au(111) Surface State Band Observed with Angle Resolved Photoelectron Spectroscopy, Phys. Rev. Lett. **77**, 3419 (1996).

[2] F. Reinert, G. Nicolay, S. Schmidt, D. Ehm, and S. Hüfner, Direct measurements of the *L*-gap surface states on the (111) face of noble metals by photoelectron spectroscopy, Phys. Rev. B **63**, 115415 (2001).

[3] M. Hoesch, M. Muntwiler, V. N. Petrov, M. Hengsberger, L. Patthey, M. Shi, M. Falub, T. Greber, and J. Osterwalder, Spin structure of the Shockley surface state on Au(111), Phys. Rev. B **69**, 241401(R) (2004).

[4] S. N. P. Wissing, C. Eibl, A. Zumbülte, A. B. Schmidt, J. Braun, J. Minár, H. Ebert, and M. Donath, Rashba-type spin splitting at Au(111) beyond the Fermi level: The other part of the story, New J. Phys. **15**, 105001 (2013).

[5] R. Courths, H. Wern, U. Hau, B. Cord, V. Bachelier, and S. Hüfner, Band structure of Cu, Ag and Au: Location of direct transitions on the Λ line using angle-resolved photoelectron spectroscopy (ARUPS), J. Phys. F **14**, 1559 (1984).

[6] P. Heimann, H. Miosga, and H. Neddermeyer, Occupied Surface-State Bands in *sp* Gaps of Au(112), Au(110), and Au(100) Faces, Phys. Rev. Lett. **42**, 801 (1979).

[7] M. Sastry, K. C. Prince, D. Cvetko, A. Morgante, and F. Tommasini, Photoemission investigation of the reconstructed Au(110) surface, Surf. Sci. **271**, 179 (1992).

[8] A. Nuber, M. Higashiguchi, F. Forster, P. Blaha, K. Shimada, and F. Reinert, Influence of reconstruction on the surface state of Au(110), Phys. Rev. B **78**, 195412 (2008).

[9] D. G. Fedak and N. A. Gjostein, A low energy electron diffraction study of the (100), (110) and (111) surfaces of gold, Acta Metall. **15**, 827 (1967).

[10] R. Feder, N. Müller, and D. Wolf, Spin polarization in low-energy electron diffraction from Au(110): Theory and experiment, Z. Phys. B **28**, 265 (1977).

[11] W. Moritz and D. Wolf, Structure determination of the reconstructed Au(110) surface, Surf. Sci. **88**, L29 (1979).

[12] P. Heimann, J. F. van der Veen, and D. E. Eastman, Structure-dependent surface core level shifts for the Au(111), (100), and (110) surfaces, Solid State Commun. **38**, 595 (1981).

[13] G. Binnig, H. Rohrer, C. Gerber, and E. Weibel, Surface Studies by Scanning Tunneling Microscopy, Phys. Rev. Lett. **49**, 57 (1982).

[14] R. A. Bartynski and T. Gustafsson, Experimental study of surface states on the (110) faces of the noble metals, Phys. Rev. B **33**, 6588 (1986).

[15] R. Drube, V. Dose, H. Derks, and W. Heiland, The 1×1 to 1×2 phase transition of Au(110): An inverse photoemission study, Surf. Sci. **214**, L253 (1989).

[16] M. Nagano, A. Kodama, T. Shishidou, and T. Oguchi, A first-principles study on the Rashba effect in surface systems, J. Phys.: Condens. Matter **21**, 064239 (2009).

[17] E. Simon, A. Szilva, B. Ujfalussy, B. Lazarovits, G. Zarand, and L. Szunyogh, Anisotropic Rashba splitting of surface states from the admixture of bulk states: Relativistic *ab initio* calculations and $k \cdot p$ perturbation theory, Phys. Rev. B **81**, 235438 (2010).

[18] G. N. Derry, M. E. Kern, and E. H. Worth, Recommended values of clean metal surface work functions, J. Vac. Sci. Technol. A **33**, 060801 (2015).

[19] S. D. Stolwijk, H. Wortelen, A. B. Schmidt, and M. Donath, Rotatable spin-polarized electron source for inverse-photoemission experiments, Rev. Sci. Instrum. **85**, 013306 (2014).

[20] C. Thiede, I. Niehues, A. B. Schmidt, and M. Donath, The acetone bandpass detector for inverse photoemission: operation in proportional and Geiger–Müller modes, Meas. Sci. Technol. **29**, 065901 (2018).

[21] M. Budke, V. Renken, H. Liebl, G. Rangelov, and M. Donath, Inverse photoemission with energy resolution better than 200 meV, Rev. Sci. Instrum. **78**, 083903 (2007).

[22] A. Zumbülte, A. B. Schmidt, and M. Donath, Momentum resolution in inverse photoemission, Rev. Sci. Instrum. **86**, 013908 (2015).

[23] T. Okuda, K. Miyamaoto, H. Miyahara, K. Kuroda, A. Kimura, H. Namatame, and M. Taniguchi, Efficient spin resolved spectroscopy observation machine at Hiroshima Synchrotron Radiation Center, Rev. Sci. Instrum. **82**, 103302 (2011).

[24] T. Okuda and A. Kimura, Spin- and Angle-Resolved Photoemission of Strongly Spin–Orbit Coupled Systems, J. Phys. Soc. Jpn. **82**, 021002 (2013).

[25] P. Eickholt, C. Sanders, M. Dendzik, L. Bignardi, D. Lizzit, S. Lizzit, A. Bruix, P. Hofmann, and M. Donath, Spin Structure of *K* Valleys in Single-Layer WS_2 on Au(111), Phys. Rev. Lett. **121**, 136402 (2018).

[26] Since we probe the surface state in its flat part of the parabolic dispersion, it is justified to fit the data with one Lorentzian line

instead of a sum of lines at slightly different energies to account for the experimental angular resolution.

[27] W. Altmann, V. Dose, and A. Goldmann, Momentum-resolved bremsstrahlung isochromat spectroscopy of silver surfaces, Z. Phys. B **65**, 171 (1986).

[28] W. Jacob, V. Dose, U. Kolac, T. Fauster, and A. Goldmann, Bulk, surface and thermal effects in inverse photoemission spectra from Cu(100), Cu(110) and Cu(111), Z. Physik B: Condens. Matter **63**, 459 (1986).

[29] The decrease of intensity with increasing angles of electron incidence θ is caused by the photon-emission characteristics (dipole axis) of the surface state. Our photon counter is positioned at $(\alpha_{\theta=0^\circ}, \beta) = (65^\circ, 32^\circ)$ relative to the electron beam, where α and β denote the polar and azimuth angle of photon detection, respectively. As θ increases the sample is rotated towards the photon detector, thereby decreasing the angle of photon detection, and hence the measured intensity decreases due to the orientation of the dipole axis. This is different from Ref. [15], where a mirror spectrometer was used and the intensity did not decrease for larger angles.

[30] To account for the different angular resolutions in ARPES and SARPES, we simulated spin-integrated SARPES spectra by a convolution of ARPES line scans (not shown). The weight factors for the line scans were taken from a Gaussian distribution, whose width is defined by the angular resolution in SARPES. The spectra obtained show the same behavior as observed in our SARPES data: (i) broadened features and (ii) increased intensities at E_F.

[31] J. Henk, T. Scheunemann, S. V. Halilov, and R. Feder, Magnetic dichroism and electron spin polarization in photoemission: Analytical results, J. Phys.: Condens. Matter **8**, 47 (1996).

[32] C. Jozwiak, Y. L. Chen, A. V. Fedorov, J. G. Analytis, C. R. Rotundu, A. K. Schmid, J. D. Denlinger, Y.-D. Chuang, D.-H. Lee, I. R. Fisher, R. J. Birgeneau, Z.-X. Shen, Z. Hussain, and A. Lanzara, Widespread spin polarization effects in photoemission from topological insulators, Phys. Rev. B **84**, 165113 (2011).